Indian Journal of Biochemistry & Biophysics
Vol. 63, October 2026, pp. 1191-1204
DOI: 10.56042/ijbb.v63i10.29103

Combined quantum-chemical and *in silico* molecular docking studies on some phytomedicinal compounds reveal potential anti-HIV leads

Avantika Pal[1] and Rahul Kumar[2]*

[1]Department of Bioinformatics, Banaras Hindu University, Varanasi-221 005, Uttar Pradesh, India
[2]Department of Zoology, Sheodeni Sao College (Magadh University), Kaler-824 127, Bihar, India

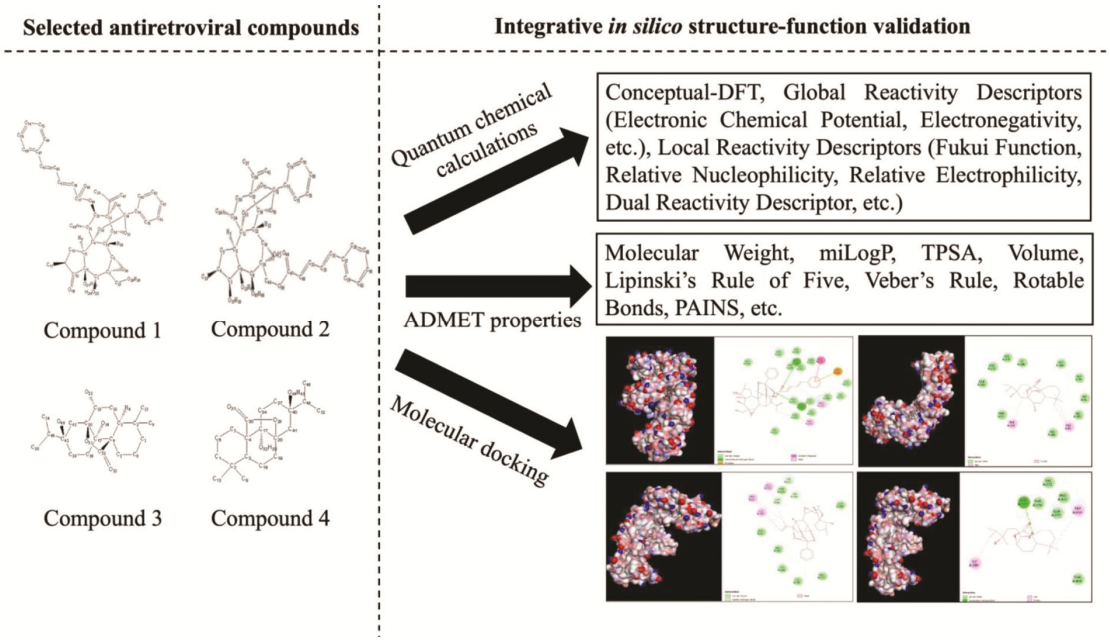
Received 24 February 2026; *revised 29 July 2026*

The human immunodeficiency virus (HIV) continues to be a global health challenge, with the emergence of drug-resistant strains highlighting the urgent need for novel therapeutics. Present work sought to examine natural diterpenoid compounds as prospective anti-HIV drugs with the objective of identifying safe and effective inhibitors that target essential HIV enzymes and viral entry mechanisms. In this study, four natural diterpenoid compounds, Onishibarin A and B (from *Daphne pseudomezereum*) and Abietamethinol C and D (from *Isodon amethystoides*) were selected based on literature survey for an integrative *in silico* structural and functional validation of their anti-HIV activities. A comprehensive cheminformatics approach involving quantum chemical calculations, *in silico* ADMET profiling, and molecular docking was employed to investigate their pharmacological potential. Geometry optimizations and reactivity descriptors were computed using density functional theory (DFT) at the B3LYP/6-31G (d,p) level to analyze their stability and electronic behavior. Global and local reactivity indices, including frontier molecular orbital energies, Fukui functions, and electrophilicity descriptors, were used to predict reactive sites and antiradical potential. ADMET assessments using SwissADME and ProTox-3.0 indicated favourable drug-likeness, low toxicity, and compliance with Lipinski's and Veber's rules. Molecular docking against HIV-1 Reverse Transcriptase (PDB ID: 3DLE) and HIV-1 gp120 Envelope Glycoprotein (PDB ID: 4RZ8) revealed strong binding affinities, especially for Onishibarin A, suggesting potential inhibitory action. Collectively, these findings support the therapeutic promise of these natural diterpenoids as leads for anti-HIV drug development and highlight the utility of integrated computational approaches in natural product-based drug discovery.

Keywords: *Daphne pseudomezereum*, Density functional theory, Diterpenoids, HIV-1, *Isodon amethystoides*, Integrase strand transfer inhibitors (INSTIs), Non-nucleoside reverse transcriptase inhibitors (NNRTIs)

Numerous illnesses and infections are brought on by viruses. Viruses are one of the biggest concerns of the healthcare system as they tend to change with time frequently and are often contagious. Almost all the human population are suffering from these insurmountable viruses. One of these viruses is HIV (human immunodeficiency virus) which leads to AIDS at its most advanced stage of infection. HIV is a retrovirus which attacks the immune system by attacking CD4+ T cells, a subset of white blood cells, which weakens the immune system[1]. It weakens defense against infections and cancers. Its advanced stage AIDS (acquired immune deficiency syndrome) results in severe illnesses such as tuberculosis, meningitis, and cancers (*e.g.*, Kaposi's sarcoma and Lymphomas). It can also lead to worsening of other infections such as Hepatitis C, Hepatitis B and Monkeypox. According to the World Health Organization, HIV remains to be a global health hazard with an estimated 44.1 million fatalities so far[2]. HIV is a retrovirus. It incorporates its genetic material into the host's genome and often mutates, making it exceptionally difficult to find a cure for this virus. HIV's replication cycle depends on a number of important viral proteins, each of which serves an essential function. In order for the virus to replicate, reverse transcriptase (RT) has to convert its single-stranded RNA into double-stranded DNA. Viral polyproteins are subsequently broken down by the protease enzyme into functional proteins needed to facilitate viral assembly. By promoting fusion between the viral envelope and the host cell membrane, the glycoproteins gp120 and gp41 promote viral entrance. Last but not least, integrase makes it possible for the viral DNA to integrate into the host genome, guaranteeing a persistent infection. These proteins work together to enable HIV infection, replication, and persistence in host cells[3,4]. Each of

*Correspondence:
E-mail: rahuldayanand33@gmail.com
Suppl. data available on respective page of NOPR



Graphical Abstract

these stages: viral entry, reverse transcription, integration, and protein maturation, offers a target for antiretroviral therapy. Drugs such as integrase strand transfer inhibitors (INSTIs), nucleoside reverse transcriptase inhibitors (NRTIs), and non-nucleoside reverse transcriptase inhibitors (NNRTIs) work by interfering with different steps of the virus's life cycle, helping to control its replication[1].

Natural products have long been useful for finding promising leads for treating a variety of illnesses. This practice has been going on for thousands of years. Many antiviral drugs consist of natural products[5,6]. From a statistical survey it was concluded that out of 185 antiviral drugs produced in the year 1981 to 2019, 28.65% were derived from natural products and natural product derivatives[7].

The exhaustive literature survey conducted in the present study highlighted that there exists a wide range of molecules in the nature of either plant or marine origin, which possess good antiretroviral/anti-HIV activity based on molecular docking studies and/or tested using a wide range of cell lines[8-25]. But the combined electronic structure calculations and *in silico* docking studies of such natural leads is an area which is yet to be explored. Nevertheless, such studies are indispensable in designing newer molecules with much better pharmacological profiles. The work done in this study is based on the idea that by following the steps listed below, we will learn more about the electronic structure properties of the studied lead molecules, as well as their reactivity and behaviour in the body, about their stability, and, finally, how well they will bind with the targeted proteins.

1. First, the data from the literature review was used to choose the lead compounds that are effective against the target proteins.
2. Information regarding the electronic structures of the molecules was computed and used to determine their reactivity (quantum-chemical calculations).
3. Molecular docking was done to check how well the lead molecule binds with the targeted protein and the efficient binding sites.
4. ADMET studies were performed to check the behaviour of the molecules in the body.
5. A pharmacophore for further drug design research was obtained by determining the structure-activity connection based on the calculations above.

Therefore, in present work an integrative approach has been employed where *in silico* structural-functional validation of antiretroviral properties has been achieved for selected compounds by combining quantum chemical calculations with *in silico* molecular docking studies.

Materials and Methods

Data Set

Based on literature survey, several of the molecules which have been extracted from various natural sources and found to possess antiviral activity are

summarised in the (Suppl. Table 1). Out of this list, four molecules were selected for present study. Among these, molecule 1 and 2 (Onishibarin A and B) belong to class diterpenoid and they target HIV-1 (NL4-3) infection in MT4 cells. These diterpenoids were extracted from the fruits of *Daphne pseudomezereum* (Thymelaeaceae) which is a deciduous shrub with light green flowers. Daphnane diterpenoids have a structure containing a highly oxygenated trans-fused ring system 5/7/6 (A/B/C) tricyclic structure[26]. Onishibarin A (compound 1) has an empirical formula of $C_{38}H_{40}O_{10}$. It has hydroxy, carbonyl, and α, β-unsaturated ester groups. It contains an orthoester carbon, isopropenyl moiety, and two methyl groups critical for its activity. There is presence of ketone group (C-3) at the A-ring and an epoxy group (C-6/C-7) at the B-ring. Resonance occurs due to presence of oxygenated functionalities. It has EC_{50} (Half Maximal Effective Concentration) of 1.26 nM and IC_{50} (Half Maximal Inhibitory Concentration) of 9.29 μM[26]. Onishibarin B (compound 2) has an empirical formula of $C_{38}H_{42}O_9$. It has similarities with compound 1 due to presence of an orthoester carbon, an isopropenyl moiety, two methyl groups, and an epoxy group. The carbonyl carbon (C-3) lacks resonance, but an oxygenated methine and methylene group do. There is also a phenyl (C-1) group present causing resonance. Furthermore O-cinnamylideneacetyl is present as the R-group. It has EC_{50} of 6.38 nM and IC_{50} of 21.0 μM[26].

Molecule 3 and 4 (Abietamethinol D and C) also belong to class diterpenoid. These compounds are known to possess anti-viral activity against Avian Influenza Virus (AIV) and Vesicular Stomatitis Virus (VSV). These were isolated from the twigs and leaves of *Isodon amethystoides,* also known as 'Wangzaozi'[27]. Abietamethinol D (compound 3) has an empirical formula of $C2_0H_{32}O_5$ which indicates five degrees of unsaturation which means the molecule has five rings and/or pi bonds, or any combination of the two. Its structure contains 7*α*, 9*α*, 13*β*-trihydroxyabiet-8, 20-lactone. It has a similar structure as compound 4 with an additional hydroxyl group. At 25μM, its antiviral inhibitory efficacy was 68.4%[27]. Abietamethinol C (compound 4) has an empirical formula of $C_{20}H_{32}O_4$ indicative of six degrees of unsaturation. It contains two angular methyl groups and resonance exhibited from an isopropyl group. It consists of a carboxyl group, three oxy-quaternary carbons, two quaternary carbons, and eight methylene groups. Its structure contains a 9*α*, 13*β*-dihydroxyabiet-8, 20-lactone. It displayed an antiviral inhibitory effect of 18.9% at 25 μM[27]. The chemical structures of the compounds are provided in (Suppl. Fig. 11).

Quantum Chemical Calculations

Electronic structure calculations involve using quantum mechanics to study the distribution of electrons in a molecule. These calculations provide insights into molecular properties, reactivity, and stability by solving Schrödinger's equation approximately for systems of interest. These calculations take input as a mechanical description of a system, which in turn give information about optical, electronic and magnetic properties. In recent times, Jelfs' density functional theory (DFT) has become increasingly useful for the understanding and calculation of the ground state density, ρ( ), and energy, E, of the molecules, clusters, and solids–any system consisting of nuclei and electrons–with or without applied static perturbations[28,29]. Within the domain of density functional theory, conceptual-DFT (or chemical reactivity theory) attempts to delineate and explicate important universal concepts of molecular structure and molecular reactivity. In this regard, global reactivity descriptors, *viz*, electronic chemical potential (denoted by μ or m), electronegativity (denoted by χ or x or c), electrophilicity index (denoted by ω or w), global hardness (denoted by η or h), global softness (S), donor index (Rd) and acceptor index (Ra) were calculated. Similarly, local reactivity descriptors, *viz*., Fukui function ($f(\vec{\boldsymbol{r}})$), local softness ($s(\vec{\boldsymbol{r}})$), relative nucleophilicity, relative electrophilicity, local electrophilicity index ($\omega(\vec{\boldsymbol{r}})$ or $w(\vec{\boldsymbol{r}})$), local hardness($\eta(\vec{\boldsymbol{r}})$ or $h(\vec{\boldsymbol{r}})$) and dual reactivity descriptor were also calculated. All these calculations are based on previous works[30-48].

All quantum chemistry computations were conducted for compounds 1, 3 and 4 using the Gaussian03X/09 software program[49]. The molecular structures of the compounds were optimised at the density functional theory (DFT) level utilising the B3LYP functional, which combines Becke's three parameter gradient-corrected hybrid exchange functional[50] with the dynamical correlation functional developed by Lee, Yang, and Parr (LYP)[51]. All computations were conducted without any symmetry constraints. Comprehensive calculations were conducted at the HF/3-21G, B3LYP/3-21G, and

B3LYP/6-31G(d,p) theoretical levels, focusing on the computed energy (ESCF: Self-Consistent Field Energy) and the associated computational expenses for the analysis of these systems. All atoms were characterised using the standard 6-31G(d,p) basis set[52], which encompasses adequate basis functions to represent the molecular characteristics of the compounds. The lack of imaginary frequencies in a harmonic frequency calculation conducted at the same theoretical level signifies that the computed geometry of each compound represents a genuine minimum on the potential energy surface. The optimised geometric parameters, frontier molecular orbitals, and basic vibrational frequencies were theoretically estimated using the Gaussian 03W/09 software package. Numerous thermochemical parameters, including zero-point vibrational energy, thermal energy, thermal enthalpy, and thermal entropy, have been computed for all substances at the same theoretical level. The atomic charges for all atoms in the selected compounds for this investigation were computed utilising Mulliken Population Analysis (MPA), Hirshfeld Population Analysis (HPA), and Natural Population Analysis (NPA) at an equivalent theoretical level. The energy of frontier molecular orbitals has been calculated using finite difference approximation where single point energy calculation was performed for the neutral (N), cation (N-1) and anion (N+1) systems of each compound of the data set and Koopman's approximation[53,54]. The conceptual DFT based global reactivity descriptors, *viz*., electronic chemical potential, electronegativity, chemical hardness, global softness and electrophilicity index have been calculated for all the compounds of the data set, using finite difference approximation. Local reactivity descriptors derived from conceptual DFT, including Fukui functions, local softness, local hardness, local electronegativity, relative nucleophilicity, relative electrophilicity, and dual descriptors, have been computed for the designated atoms of all compounds, based on the aggregated findings of *in vitro* biological activity. The molecule electrostatic potential maps and the visualisation of the results were conducted using Gauss View 5.0.[55]. Note that compound 2 was optimized only at the HF/3-21G level because of computational limitations (high computational cost with highest number optimization steps) as shown in the results and discussion section. Therefore, DFT-based electronic structure analyses (B3LYP/6-31G(d,p)) were performed only for compounds 1, 3, and 4, while compound 2 was included in all ADMET and molecular docking studies.

Selection of antiviral targets

HIV-1 reverse transcriptase (PDB ID: 3DLE) and envelope glycoprotein (PDB ID: 4RZ8) were selected as antiviral targets for molecular docking studies. HIV-1 Reverse Transcriptase (abbreviated HIV-1 RT) is a heterodimer enzyme that has a major role in virus replication. The heterodimer structure consists of two subunits p66 and p51 which act as distinct inhibitor sites where p66 binds nucleotide analogue inhibitors (NRTIs) and p51 binds non-nucleoside inhibitors (NNRTIs). HIV-1 RT is susceptible to mutations leading to drug resistance. Thus, there's a need to come up with novel drugs that are active against mutated HIV as well[56]. HIV-1 Envelope Glycoprotein (abbreviated HIV-1 gp120) is a surface glycoprotein essential for the viral entry by binding to the host CD4 receptors. This causes conformational changes in gp120 leading to its interaction with host cell co-receptors CCR5 or CXCR4. Currently there are no drugs available in the market aiming at HIV-1 gp120[57].

Computer aided drug designing (CADD) studies

In silico ADMET studies

In silico ADMET studies for all the compounds of the data set have been carried out using open source web program Swiss ADME (http://www.swissadme.ch/citing.php) and ProTox-3.0 (https://tox.charite.de/protox3/). These programs allow us to predict ADMET (absorption, distribution, metabolism, excretion, and toxicity) properties as well as physiochemical properties, lipophilicity, pharmacokinetics, drug-likeness, medicinal chemistry, and predicted toxicity of a drug to aid with drug discovery[58,59]. For giving input, OpenBabel GUI version 2.4.1 software (https://sourceforge.net/projects/openbabel/) was used to generate SMILES notation for each compound[60]. The generated SMILES notation was then used to calculate molecular properties like Log P, Total polar surface area (TPSA), number of hydrogen bond donors and acceptors, molecular weight, number of atoms, number of rotatable bonds, Lipinski's rule violations, Veber's rule violation, and predicted toxicity (Table 1). The molecular properties calculated are described below:

Table 1 — SMILES notations of the selected compounds (1-4)

Molecule No.	SMILES Notation
1	[C@H]1([C@@]2([C@@H](O2)[C@@H]2[C@@]3([C@H]4[C@]1(C(=O)[C@H](C4)C)O)[C@@H]([C@H](C@]1([C@@H]2O[C@](O1)(O3)c1ccccc1)C(=C)C)OC(=O)/C=C\C=C/c1ccccc1)C)CO)O
2	[C@@H]1([C@H](C[C@@H]2[C@@]31[C@H]([C@@]1([C@@H]([C@@H]4[C@@]52[C@H](C)C[C@]2([C@@H]4O[C@@](O5)(O2)c2ccccc2)C(=C)C)O1)CO3)O)C)O.C(=O)(O)/C=C/C=C/c1ccccc1
3	C1C([C@H]2[C@]3(CC1)[C@@]1([C@]([C@@H](C2)O)(OC3=O)C[C@@](CC1)(O)C(C)C)O)(C)C
4	C1C([C@H]2[C@]3(CC1)[C@@]1([C@](CC2)(OC3=O)C[C@@](CC1)(O)C(C)C)O)(C)C

(i) miLogP (octanol/water partition coefficient): The archetype of the topological technique forecasts a linear correlation with thirteen chemical descriptors.

(ii) Molecular Polar Surface Area (TPSA): TPSA is determined by aggregating the contributions of polar fragments containing oxygen and nitrogen[61]. TPSA is an excellent descriptor for characterising drug absorption, encompassing intestinal absorption, bioavailability, Caco-2 permeability, and blood-brain barrier penetration.

(iii) Molecular volume: The volume of a molecule is determined based on group contributions. These were derived by fitting a summation of fragment contributions to an actual 3D volume for a training set of approximately twelve thousand predominantly drug-like compounds.

(iv) "Rule of 5" properties: This refers to a collection of fundamental molecular descriptors utilised by Lipinski in the development of his "Rule of 5". The guideline specifies that the majority of " drug-like" compounds possess a logP $\leq$ 5, a molecular weight $\leq$ 500, a maximum of 10 hydrogen bond acceptors, and a maximum of 5 hydrogen bond donors. Molecules that contravene multiple rules may encounter issues with bioavailability.

(v) Veber's Rule posits that a molecule must possess a polar surface area (PSA) of $\leq$ 140 Å² and no more than 10 rotatable bonds to exhibit favourable oral bioavailability[62]. (vi) Rotable Bonds: This fundamental topological characteristic quantifies molecular flexibility. It has been demonstrated to be an excellent indicator of the oral bioavailability of pharmaceuticals[62]. A rotable bond is characterised as any singular non-cyclic bond attached to a non-terminal heavy atom (*i.e.*, not hydrogen). Amide C−N bonds are excluded due to their elevated rotational energy barrier.

(vii) PAINS: It denotes Pan Assay Interference Compounds. It comprises compounds with substructures that demonstrate a robust reaction when the protein target is excluded from the assay.

Drug likeness may be defined as a complex balance of various molecular properties and structure features which determine whether a particular molecule is similar to the known drugs. The properties of hydrophobicity, electronic distribution, hydrogen bonding characteristics, molecular size and flexibility, as well as the presence of diverse pharmacophoric features, significantly influence molecular behaviour in living organisms, encompassing bioavailability, transport properties, protein affinity, reactivity, toxicity, metabolic stability, and more.

In silico molecular docking studies

The binding affinities between the ligands (selected 4 compounds) and the receptors (HIV-1 Reverse Transcriptase and Envelope Glycoprotein gp120) have been studied through docking studies, using the Autodock 4.0[63], PyRx 0.8[64] and an online server of docking, SwissDock. The docking results were analyzed with the help of Biovia Discovery Studio 2025 (https://discover.3ds.com/discovery-studio-visualizer-download). To examine the interaction of selected compounds as mentioned in (Suppl. Fig. 11) to the reported targets namely HIV-1 Reverse Transcriptase and Envelope Glycoprotein gp120 from the Protein Data Bank (PDBid:3DLE and PDBid:4RZ8 respectively) (www.rcsb.pdb),docking simulation were carried by using AutoDock 4.0 program of MGL Tool 1.5.7 software (https://ccsb.scripps.edu/mgltools/downloads/), Pyrx 0.8 (https://sourceforge.net/projects/pyrx/) and SwissDock (https://www.swissdock.ch). The steps for conducting the Molecular Docking studies using AutoDock 4.0 are as follows:

Protein Optimization

In protein optimization, the protein (PDB id - 3DLE and 4RZ8) was prepared for running docking simulation. The resolution of the protein is 2.50 Å and 1.90 Å, respectively. For docking the inhibitor is removed from the protein and energy is minimized.

Preparation for molecular docking

The procedure preceding molecular docking consists of the following steps:

(i) Protein preparation: The co-crystallized ligand structure and hydrogen atoms were eliminated utilising AutoDock 4.0 software. Subsequently, the Kollman charges were incorporated into each atom, together with AD4 charges and polar hydrogen atoms, into the protein structure. The structures were subsequently stored in PDBQT file format for input into AutoDock version 4.0.

(ii) Ligand preparation: An optimised Gauss log file was utilised to create a 3D PDB file from its 2D representation using Open Babel software (O'Boyle *et al*. 2011), and subsequently saved in (.pdb) file format for input into AutoDockTools (ADT) version 1.5.Seven. Subsequently, all ligand structures were preserved in PDBQT file format following the identification and selection of the root, for input into AutoDock version 4.0.

(iii) Grid formation: The protein molecule and ligand were selected in .pdbqt format, and the grid box was established in the target proteins (3DLE and 4RZ8), thereafter saving the file in .gpf format (grid parameter file).

(iv) Docking preparation: The protein and ligand were selected in pdbqt file format, and the file was subsequently saved in .dpf format (docking parameter file) utilising default parameters (GA runs = 10; population size = 150, *etc*.).

Running docking algorithm

For running docking algorithms Cygwin (http://www.cygwin.com/) were used, .glg and .dlg files were created from the grid file .gpf and .dpf file respectively. The commands for executing autogrid and autodock were "./autogrid4.exe –p lig.gpf –f lig.glg &" and "./autodock"4.exe –p lig.dpf –f lig.dlg & Cygwin was executed once more to convert the .dlg file into a run.pdbqt file, which was subsequently executed. The pdbqt files were transformed into run.pd.b. The optimal ligand with the lowest binding energy was identified from the .dlg file, and its coordinates were extracted from the .run.pdb file to be inserted into the protein optimisation file. The file has been saved in the .pdb format.

Visualization of docked protein

Biovia Discovery Studio 2025 was used for visualization of hydrogen bond interaction between protein and ligand molecule, electrostatic interaction, 2D structure, 3D structure and pose organizer view of ligand that shows in which conformation the ligand is bound stably with protein structure.

Results and Discussion

Electronic structure calculations

Predicting ability of theoretical method

The DFT-based quantum chemical calculations on compounds 1, 3 and 4, as indicated in (Suppl. Fig. 11), were successfully conducted in the gas phase with various functionalities, as detailed in the computational section. All parameters exhibit identical divergence, as evidenced by the data presented in (Suppl. Table 2), Hartree-Fock (HF), and DFT. The minimal energy structure of all molecules was found at the DFT functional level. The lowest absolute value of ESCF corresponds to the optimised structure of the study (compound 1, 3 and 4). The highest ESCF energy is achieved in compound 1. Compound 4 exhibits the highest dipole moment.

The effect of the basis set

The computations for all examined chemicals, as indicated in (Suppl. Fig. 11), have been successfully conducted in the gas phase using various combinations of basis sets, as detailed in (Suppl. Table 2). There are three basis sets: the first is HF, specifically HF/3-21G, and the two DFT methods are B3LYP/3-21G and B3LYP/6-31G(d, p). All groups of molecules exhibit minimal optimisation energy, low dipole moments, high computational costs, and a constant reduction in the number of optimisation steps throughout each group.

Computational cost

In quantum-chemical calculations an important criterion for the relevancy of the DFT is availability or computational time is needed. The CPU time for optimising the molecule is given in (Suppl. Table 2). Suppl. Table 2 clearly demonstrates that the computing cost escalates with the enhancement of the level of theory and the basis set. The computing cost was contingent upon the number of atoms and the characteristics of the atoms within the molecule. The largest computational cost of compound 1 arises from the existence of 10 oxygen atoms and 5 rings, whereas the minimum cost of compound 3 is attributed to its lower atom count and the presence of 4 oxygen atoms. Compound 2 has high computational cost with highest number of optimization steps among all four compounds, making it difficult to optimize it beyond HF/3-21G level.

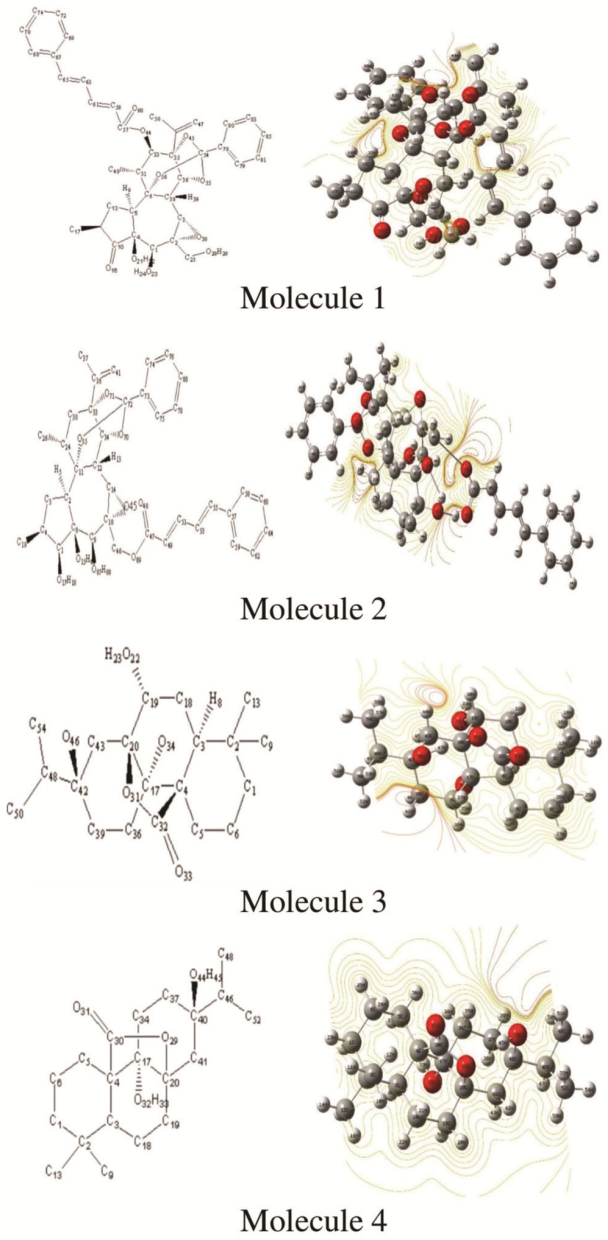


Fig. 1 — Ground state optimized geometry structure with contour plots in gas phase for selected compounds (1, 3, and 4) calculated at B3LYP/6-31G(d,p) level of theory. Molecule 2 optimized at HF/3-21G; 1 and 4 optimized at B3LYP/3-21G level of theory.

Geometry optimization

The geometry optimisation of all examined compounds was conducted using DFT at the B3LYP/3-21G/B3LYP/6-31G(d, p) theoretical level. When the values of the four parameters (Maximum Force, Maximum Displacement, RMS Force, and RMS Displacement) exceed their threshold values, we conclude that the compound is optimised. Figure 1 displays the optimised structures of compounds 1-4 together with their contour plots.

Thermochemical studies

The energetic and thermochemical parameters for compounds 1, 3 and 4 in the gas phase at 1 atm and 298.15 K, calculated using HF/3-21G, B3LYP/3-21G, and B3LYP/6-31G(d,p) methods, are detailed in (Suppl. Table 3). The zero-point vibrational energy (ZPVE) is the energy differential of the ground state's vibrational mode. The zero-point vibrational energy of molecule 1 is elevated compared to the other compounds. Additionally, the total energy of all examined compounds has been computed in the gas phase following zero-point and thermal corrections to energy, enthalpy, and Gibbs free energy. The results presented in (Suppl. Table 3) demonstrate that all researched compounds are exothermic.

Atomic Charges

Atomic charges have been calculated by three different population analyses; MPA (Mulliken population analysis), and HPA (Hirshfeld population analysis) and NPA (Natural population analysis) of compounds 1-4. The results are given in Appendices 1, 2 and 3 respectively. The plot of atomic charges is also given in (Fig. 2) for MPA, HPA & NPA. In compound 1, atoms C23 and C54 has maximum population for neutral, anion and cation on the basis of NPA and atom C1 has minimum. Molecular structure and charge of compound 2 is almost similar to compound 1. In compound 3, C32 has maximum and C19 has minimum population for neutral, anion and cation based on NPA. In compound 4, C30 has maximum and C20 has minimum population for neutral, anion and cation based on NPA.

Molecular electrostatic potential (MEP)

MEP maps also known as electrostatic potential maps are a 3-D representation of the molecule. The colour of the map gives information about electron rich and electron poor regions in the molecule, where blue zones represent good nucleophilic sites, red zones represent good electrophilic sites, and green zones are electrically neutral. MEP plots of all the studied compounds are shown in (Fig. 3).

Antiradical Capacity

Antiradical activity of a compound may be evaluated from the oxidation and reduction potential that is based on ionization potential (*I*) and electron affinity *(A)*, respectively. A molecule with a low value of *I* is easily oxidised, therefore, a good electron

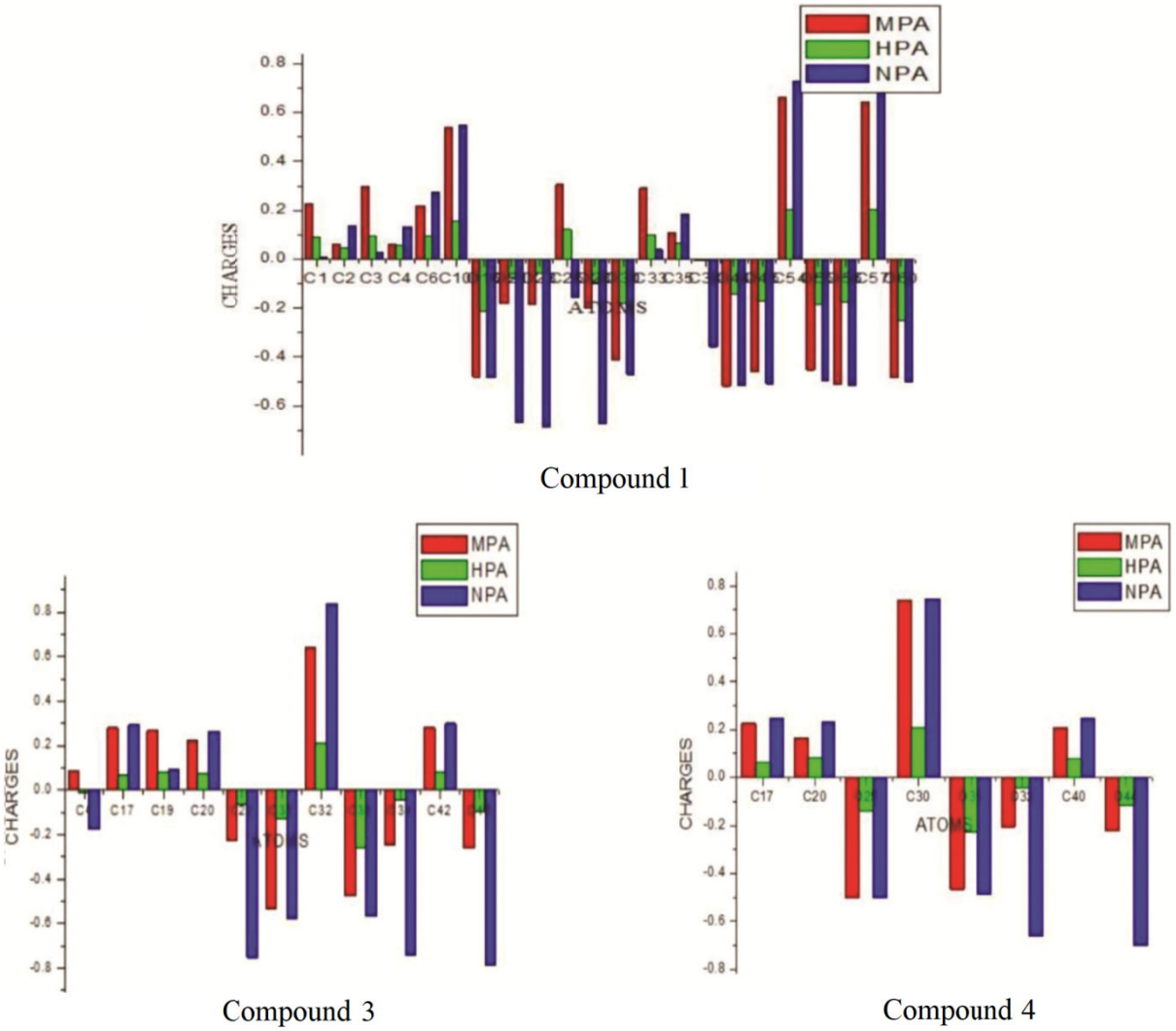


Fig. 2 — Variation of atomic charges at the selected atoms (k) of (compounds 1, 3 and 4) based on NPA, MPA and HPA calculated at B3LYP/6-31G(d, p) level of theory. Molecules 1 and 4 optimized at B3LYP/3-21G level of theory. Note that molecular structure and charge of compound 2 is almost similar to compound 1. Therefore, compound 2 is not shown here

donor. On the other hand, a molecule with a high value of E is a good electron acceptor. Antiradical capacity of all studied compounds is represented in (Suppl. Table 4). The ionisation potential of compound 4 is high so it acts as an antioxidant, and compound 1 has high electron affinity so, so compound 1 shows a good anti-redundant.

Frontier molecular orbital analysis and conceptual DFT based global reactivity Descriptors

The Highest Occupied Molecular Orbital (HOMO) and Lowest Unoccupied Molecular Orbital (LUMO) with their band gap ($\Delta E = E_{LUMO} - E_{HOMO}$) is shown in (Fig. 4). The calculated frontier molecular orbital energies, energy band gap, energy of neutral, anion and cation on the basis of NPA, dipole moment, electronic chemical potential, electronegativity, global hardness, global softness, and electrophilicity index at B3LYP/3-21G/B3LYP/6-31G(d, p) level of theory presented in the (Suppl. Table 5). The dipole moment of compound 3, measuring 4.5148 Debye, indicates a more pronounced charge separation inside the complex. Compound 1 has the lowest energy band gap, while compound 4 displays the highest, indicating the relative softness and hardness of the molecules, respectively. Compound 1 exhibits a superior electrophilicity index relative to others, indicating that these two compounds possess an enhanced propensity to take electrons.

Conceptual DFT-based local descriptors

The local descriptors such as Fukui function, local softness, local electrophilicity, local hardness, relative

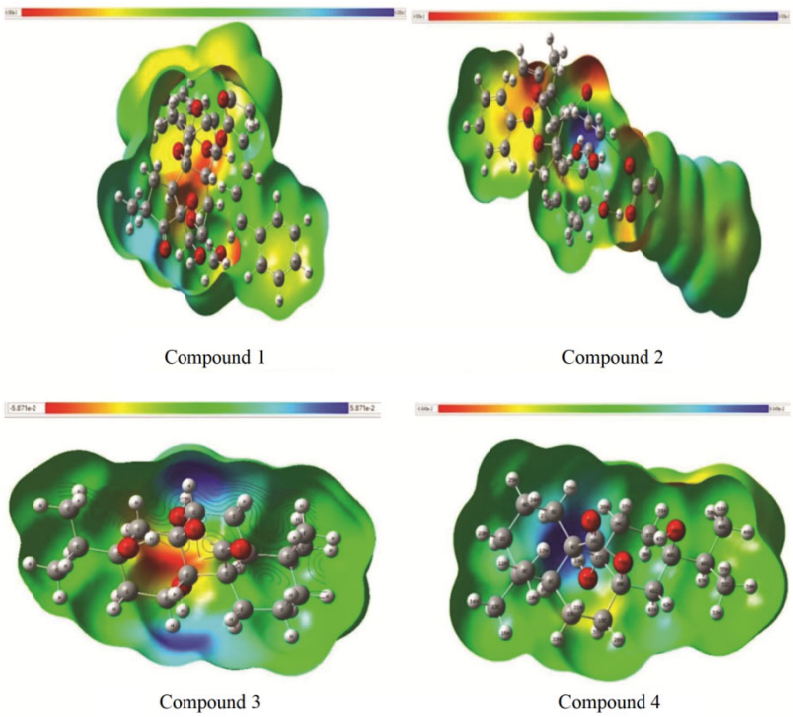


Fig. 3 — Molecular electrostatic potential (MEP) plot of the ground state optimized geometry (in gas phase) for compound (1-4) calculated at B3LYP/6-31G(d,p) level of theory. Molecule 2 optimized at HF/3-21G; 1 and 4 optimized at B3LYP/3-21G level of theory.

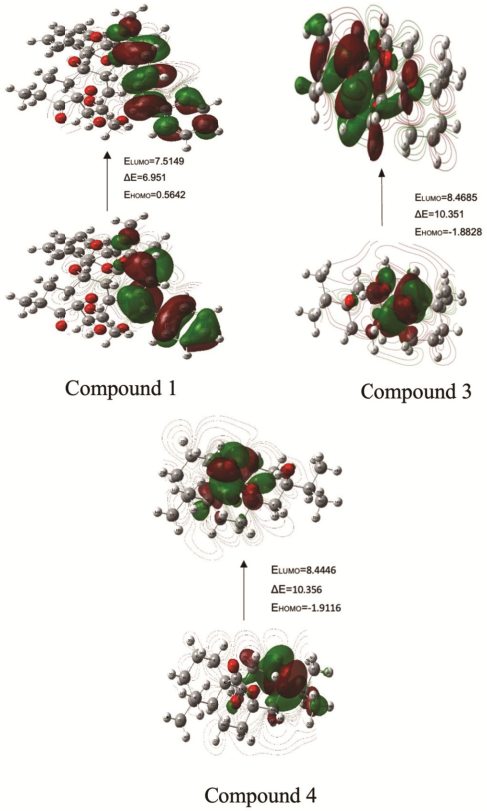


Fig. 4 — HOMO and LUMO plots along with the band gap (ΔE) for compound (1, 3 and 4), calculated at B3LYP/6-31G(d,p) level of theory. Molecules 1 and 4 optimized at B3LYP/3-21G level of theory.

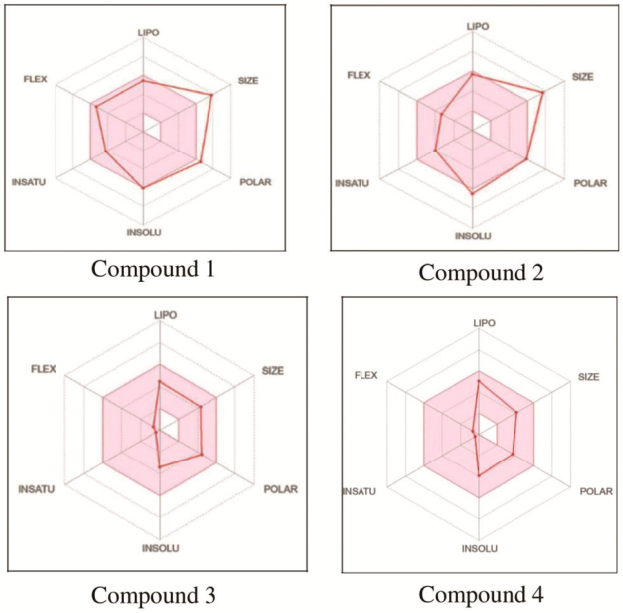


Fig. 5 — Diagrammatic representation of the bioavailability radar of the compounds (1-4). The coloured zone is the suitable physicochemical space for oral bioavailability

electrophilicity, relative nucleophilicity, and dual descriptor are presented in (Appendix 4 and Suppl. Figs. 1-11). The calculated local reactivity descriptors in Appendix 4 for the set of studied compounds show different reactive sites for each molecule. Under MPA,

Table 2 — ADMET result for all the studied compounds (1-4) using Swiss ADMET and ProTox software

Molecule No.	1	2	3	4
MW (g/mol)	656.72	642.73	352.47	336.47
TPSA(Å^2)	144.28	127.21	86.99	66.76
H-bond Acceptors	10	9	5	4
H-bond donors	3	3	3	2
Rotatable Bonds	8	5	1	1
milogP	2.00	2.84	2.18	2.91
Lipinski's Violations	1	1	0	0
Veber's Violations	1	0	0	0
GI Absorption	Low	Low	High	High
BBB permeant	No	No	No	Yes
Bioavailability Score	0.55	0.56	0.55	0.55
PAINS (Pan Assay Interference Structures)	0	0	0	0
Predicted LD50 (mg/kg)	590	400	15900	15900
Predicted Toxicity Class	4	5	6	6
Average Similarity(%)	56.5	56.51	83.62	85.29
Prediction Accuracy(%)	67.38	67.38	70.97	70.97

compound 1 presents its maximum electrophilic and nucleophilic Fukui functions (f^+ = 0.0362 a.u., f^- = 0.0649 a.u.), local softness (s^+ = 0.0052 a.u., s^-= 0.0093 a.u.), and local electrophilicity (w^+ = 0.0425 a.u., w^- = 0.0762 a.u.) at atom O60, while atom C10 has the highest relative nucleophilicity (8.2407) and dual descriptor (1.0640), atom C25 has the highest relative electrophilicity (2.3372), and atom C57 has the highest local hardness ($D^+h(k)$ = -0.1138 a.u.). For compound 3, the maximum Fukui function (f^+ = 0.0742 a.u., f^- = 0.2003 a.u.), local softness (s^+ = 0.0072 a.u., s^- = 0.0193 a.u.), and local electrophilicity (w^+ = 0.0645 a.u., w^- = 0.1741 a.u.) occur at atoms O22 (f^+, s^+, w^+) and C32 (f^-, s^-, w^-), with C32 also showing the highest relative nucleophilicity (7.6450) and dual descriptor (4.7375), atom O46 achieving the highest relative electrophilicity (5.0148), and atom O46 holding the highest local hardness ($D^+h(k)$ = -0.1823 a.u.). Finally, in compound 4, atom C40 exhibits the highest f^+ (0.0584 a.u.), s^+ (0.0056 a.u.), w^+ (0.0301 a.u.), and relative electrophilicity (3.7498), whereas atom C30 shows the maximum f^- (0.2108 a.u.), s^- (0.0204 a.u.), w^- (0.1086 a.u.), relative nucleophilicity (7.4050), and dual descriptor (4.9610), with the highest local hardness recorded at atom O44 ($D^+h(k)$ = -0.2256 a.u.). In simple terms, these results reveal the specific "hotspots" on each molecule that dictate how and where they will react with other chemical compounds. In compound 1, the oxygen atom O60 is the most active overall center for gaining or losing electrons, while carbon C10 is best suited for attracting electron-seeking agents and carbon C25 excels at attracting electron-donating agents. Compound 3 operates through two main centers: oxygen O22 acts as the primary site for accepting electrons, whereas carbon C32 is the most dominant site for donating electrons, driving general chemical preference, and attacking positive targets. Finally, compound 4 divides its responsibilities between two key carbons, where carbon C40 acts as the main center for attracting electron-rich species, and carbon C30 serves as the primary engine for donating electrons and driving nucleophilic reactions (Suppl. Figs. 1-11).

In silico ADMET studies

The *In silico* ADMET studies involve calculation of physico-chemical properties (Absorption, Distribution, Metabolism, Excretion and Toxicity) and drug-likeness of a drug which are calculated using SwissADME and ProTox software. The results for the studied compounds (1-4) are presented in (Table 2) and the bioavailability RADARS are presented in (Fig. 5). From the output obtained it can be stated that compounds 1 and 2 does not possess good ADMET properties due to 1 Lipinski's rule violation each (High molecular weight), low GI absorption and moderate toxicity whereas compounds 3 and 4 displayed good ADMET results due to compliance with drug likeness criteria, high GI absorption and low toxicity.

In silico molecular docking studies

The *in silico* docking studies have been done against different cytotoxic compounds based on their docked

Table 3 — Molecular docking results for all the studied molecules (1-4) using AutoDock

HIV-1 Reverse Transcriptase (3DLE)

Molecule	Estimated Free Energy of Binding (kcal/mol)	Estimated Inhibition Constant (μM)	Final Intermolecular Energy (kcal/mol)	Van der Waals + H bond + dissolved Energy (kcal/mol)	Electrostatic Energy (kcal/mol)	Final Total Internal Energy (kcal/mol)	Torsional Free Energy (kcal/mol)	Unbound System's Energy (kcal/mol)
OnishibarinA	-7.53	3.00	-10.82	-10.67	-0.15	-5.68	+3.28	-5.68
Onishibarin B	-5.88	48.83	-8.86	-7.17	-1.69	-0.22	+2.98	-0.22
AbietametinolD	-6.84	9.66	-8.03	-8.00	-0.04	-1.54	+1.19	-1.54
Abietamethinol C	-6.41	20.11	-7.30	-7.23	-0.07	-0.86	+0.89	-0.86

HIV-1 Envelope Glycoprotein (4RZ2)

Molecule	Estimated Free Energy of Binding (kcal/mol)	Estimated Inhibition Constant (μM)	Final Intermolecular Energy (kcal/mol)	Van der Waals + H bond + dissolved Energy (kcal/mol)	Electrostatic Energy (kcal/mo l)	Final Total Internal Energy (kcal/mol)	Torsional Free Energy (kcal/mol)	Unbound System's Energy (kcal/mol)
Onishibarin A	-6.99	7.54	-10.27	-9.82	-0.45	-5.15	+3.28	-5.15
OnishibarinB	-5.88	48.83	-8.86	-7.17	-1.69	-0.22	+2.98	-0.22
Abietamethinol D	-5.82	54.00	-7.02	-6.71	-0.30	-1.96	+1.19	-1.96
Abietamethinol C	-6.76	11.05	-7.66	-7.55	-0.10	-0.84	+0.89	-0.84

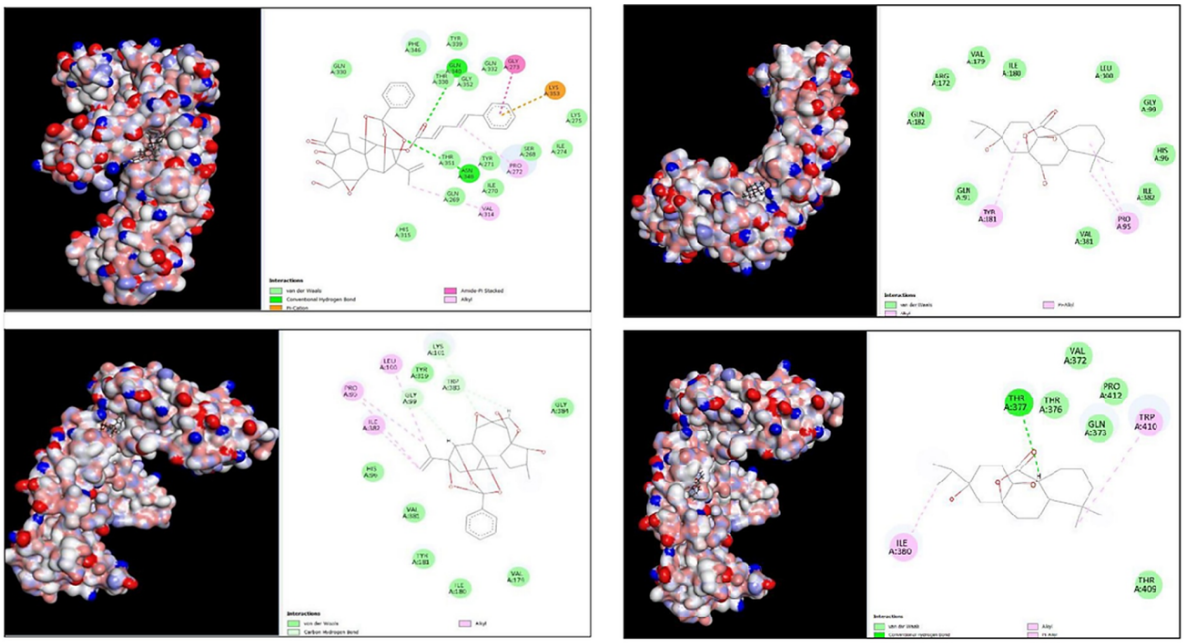


Fig. 6 — Diagrammatic representation of 3D structure and 2D structure of compounds (1-4) respectively, docked with protein 3DLE (HIV-1 Reverse Transcriptase).

on the target protein's active site (docked proteins: HIV-1 Reverse Transcriptase – 3DLE and Envelope Glycoprotein gp120 – 4RZ8). The results for the studied compounds, as presented in (Figs. 6 & 7, Table 3, and Suppl. Tables 6 & 7) indicate that all the studied compounds (1-4) show maximum binding energy with HIV-1 Reverse Transcriptase in comparison to HIV-1 Envelope Glycoprotein. Compound 1 shows the highest

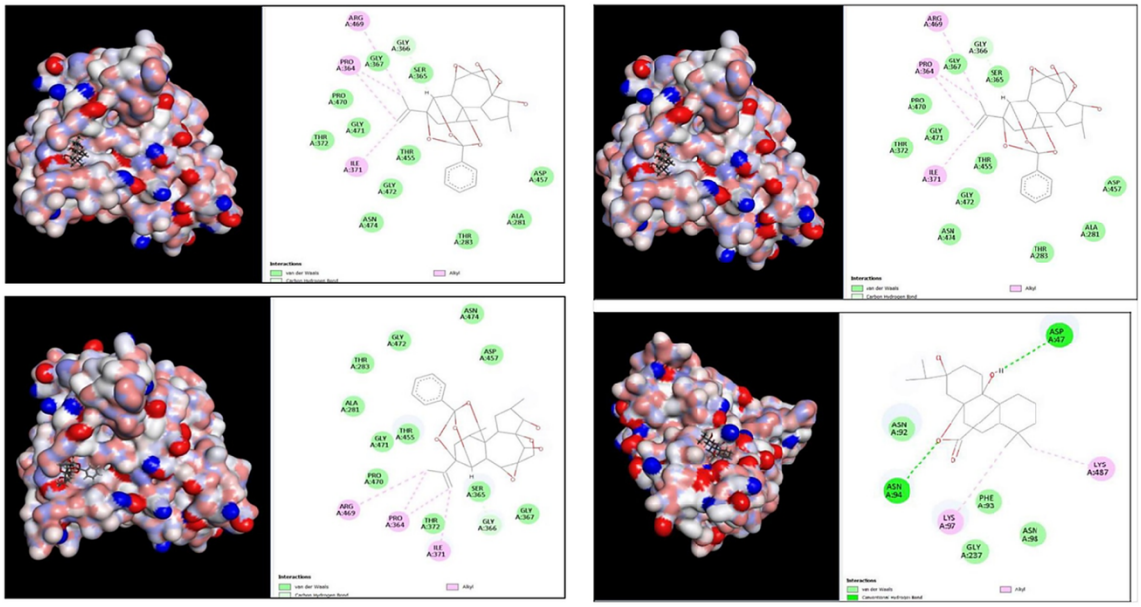


Fig. 7 — Diagrammatic representation of 3D structure and 2D structure of compounds (1-4) respectively, docked with protein 4RZ8 (HIV-1 Envelope Glycoprotein)

free energy of binding (-7.53 Kcal/mol), compound 3 shows minimum binding energy (-5.82 Kcal/mol). More negative free energy of binding obtained then that docked structure may show good interaction between ligand and target. The maximum number of hydrogen bonds obtained for compound 1 is four.

Conclusion

In this cheminformatics-based work, an integrated *in silico* approach including DFT calculations, ADMET profiling and molecular docking was employed to assess the anti-HIV potential of four natural diterpenoid compounds, Onishibarin A and B (compound 1 and 2, source: *Daphne pseudomezereum*), and Abietamethinol D and C (compound 3 and 4, source: *Isodon amethystoides*). Quantum chemical calculations at the DFT B3LYP/6-31G(d,p) level provided basic information on the electronic structure, geometrical stability and reactivity parameters of the studied compounds. The global reactivity descriptors indicated that Onishibarin A had the lowest energy band gap (ΔE) and the highest electrophilicity index, suggesting its soft chemical nature and high propensity for electronic interactions. In addition, the local reactivity descriptors (Fukui functions and local softness) pointed to significant reactive hotspots on the scaffolds, especially on oxygen O60 and carbon C10/C25 in Onishibarin A, thereby defining the structural regions involved in chemical reactivity and potential receptor interactions. Pharmacokinetic and safety evaluation with SwissADME and ProTox-3.0 showed different profiles within the dataset. Abietamethinol C and D showed high gastrointestinal absorption, low toxicity, and full adherence to Lipinski's and Veber's drug-likeness rules, while Onishibarin A and B showed moderate pharmacokinetic trade-offs due to high molecular weights. Molecular docking simulations against important HIV targets revealed that all four diterpenoids bound preferentially to HIV-1 Reverse Transcriptase (RT) (PDB ID: 3DLE) rather than HIV-1 gp120 Envelope Glycoprotein (PDB ID: 4RZ8). Of these, Onishibarin A showed the most promising binding affinity (-7.53 kcal/mol), which was stabilised by strong hydrogen bonding interactions in the active site. In general, the results confirm the experimental anti-HIV activity reported in the literature and provide a clear theoretical relationship between the distribution of electronic charges, pharmacokinetic behaviour and affinity for the target. This study demonstrates the therapeutic potential of natural diterpenoids, especially Onishibarin A, as promising lead candidates for anti-HIV drug development and provides a rational computational basis for future structural optimisation and experimental validation.

Conflict of interest

All authors declare no conflict of interest.

References

1 Deeks SG, Overbaugh J, Phillips A & Buchbinder S, HIV infection. *Nat Rev Dis Primers*, 1 (2015) 15035.

2 World Health Organization, HIV and AIDS [Internet]. Geneva: World Health Organization; 2025 [cited 2025 Jul 27]. Available from: https://www.who.int/news-room/fact-sheets/detail/hiv-aids.

3 Laskey SB & Siliciano RF, A mechanistic theory to explain the efficacy of antiretroviral therapy. *Nat Rev Microbiol*, 12 (2014) 772.

4 Ng TB, Huang B, Fong WP & Yeung HW, Anti-HIV agents from higher plants. *Life Sci*, 61 (1997) 933.

5 Kitazato K, Wang Y & Kobayashi N, Viral infectious disease and natural products with antiviral activity. *Drug Discov Ther*, 1 (2007) 14.

6 Lin LT, Hsu WC & Lin CC, Antiviral natural products and herbal medicines. *J Tradit Complement Med*, 4 (2014) 24.

7 Kim EA, Kang N, Heo JH, Park A, Heo SY, Kim HS & Heo SJ, Antiviral activity of *Ecklonia cava* extracts and dieckol against Zika virus. *Int J Mol Sci*, 25 (2024) 13694.

8 Asada Y, Sukemori A, Watanabe T, Malla KJ, Yoshikawa T, Li W, Koike K, Chen CH, Akiyama T, Qian K, Nakagawa-Goto K, Morris-Natschke SL & Lee KH, Stelleralides A-C, novel potent anti-HIV daphnane-type diterpenoids from *Stellera chamaejasme* L. *Org Lett*, 13 (2011) 2904.

9 Cheng YY, Chen H, He HP, Zhang Y, Li SF, Tang GH, Guo LL, Yang W, Zhu F, Zheng YT, Li SL & Hao XJ, Anti-HIV active daphnane diterpenoids from *Trigonostemon thyrsoideum*. *Phytochemistry*, 96 (2013) 360.

10 Liu YY, Liu YP, Wang XP, Qiao ZH, Yu XM, Zhu YZ, Xie L, Qiang L & Fu YH, Bioactive daphnane diterpenes from *Wikstroemia chuii* with their potential anti-inflammatory effects and anti-HIV activities. *Bioorg Chem*, 105 (2020) 104388.

11 Otsuki K, Li W, Asada Y, Chen CH, Lee KH & Koike K, Daphneodorins A-C, anti-HIV daphnane diterpenoids from *Daphne odora*. *Org Lett*, 22 (2019) 11.

12 Zhang X, Huang SZ, Gu WG, Yang LM, Chen H, Zheng CB, Zhao YX, Wan DCC & Zheng YT, Wikstroelide M potently inhibits HIV replication by targeting reverse transcriptase and integrase nuclear translocation. *Chin J Nat Med*, 12 (2014) 186.

13 Yan M, Lu Y, Chen CH, Zhao Y, Lee KH & Chen DF, Stelleralides D-J and anti-HIV daphnane diterpenes from *Stellera chamaejasme*. *J Nat Prod*, 78 (2015) 2712.

14 Otsuki K, Zhang M, Yamamoto A, Tsuji M, Tejima M, Bai ZS, Zhou D, Huang L, Chen CH, Lee KH, Li N, Li W & Koike K, Anti-HIV tigliane diterpenoids from *Wikstroemia scytophylla*. *J Nat Prod*, 83 (2020) 3584.

15 Zhang M, Otsuki K, Kikuchi T, Bai ZS, Zhou D, Huang L, Chen CH, Morris-Natschke SL, Lee KH, Li N, Koike K & Li W, LC-MS identification, isolation, and structural elucidation of anti-HIV tigliane diterpenoids from *Wikstroemia lamatsoensis*. *J Nat Prod*, 84 (2021) 2366.

16 Zhao JX, Liu CP, Qi WY, Han ML, Han YS, Wainberg MA & Yue JM, Eurifoloids A-R, structurally diverse diterpenoids from *Euphorbia neriifolia*. *J Nat Prod*, 77 (2014) 2224.

17 Zhang H, Zhu KK, Han YS, Luo C, Wainberg MA & Yue JM, Flueggether A and virosinine A, anti-HIV alkaloids from *Flueggea virosa*. *Org Lett*, 17 (2015) 6274.

18 Liu YP, Liu QL, Zhang XL, Niu HY, Guan CY, Sun FK, Xu W & Fu YH, Bioactive monoterpene indole alkaloids from *Nauclea officinalis*. *Bioorg Chem*, 83 (2019) 1.

19 Liu YP, Guo JM, Xie Z, Suo XY, Liu ZY, Qiao ZH, Guan RQ, Bian Y, Qiang L & Fu YH, Claus anisumine, a prenylated bicarbazole alkaloid from the fruits of *Clausena anisum-olens* and its potential anti-HIV activity. *J Org Chem*, 86 (2021) 17722.

20 Liu YP, Yan G, Guo JM, Liu YY, Li YJ, Zhao YY, Qiang L & Fu YH, Prenylated coumarins from the fruits of *Manilkara zapota* with potential anti-inflammatory effects and anti-HIV activities. *J Agric Food Chem*, 67 (2019) 11942.

21 Liu YP, Yan G, Xie YT, Lin TC, Zhang W, Li J, Wu YJ, Zhou JY & Fu YH, Bioactive prenylated coumarins as potential anti-inflammatory and anti-HIV agents from *Clausena lenis*. *Bioorg Chem*, 97 (2020) 103699.

22 Yu JH, Wang GC, Han YS, Wu Y, Wainberg MA & Yue JM, Limonoids with anti-HIV activity from *Cipadessa cinerascens*. *J Nat Prod*, 78 (2015) 1243.

23 Zhou X, Fang W, Tan S, Lin X, Xun T, Yang B, Liu S & Liu Y, Aspernigrins with anti-HIV-1 activities from the marine-derived fungus *Aspergillus niger* SCSIO Jcsw6F30. *Bioorg Med Chem Lett*, 26 (2016) 361.

24 Liu YP, Zhao WH, Feng XY, Zhang ZJ, Zong K, Sun ZG, Zheng YT & Fu YH, Novel tetrahydrofuran derivatives from *Trigonostemon howii* with their potential anti-HIV-1 activities. *Bioorg Chem*, 79 (2018) 111.

25 Tao L, Zhuo YT, Qiao ZH, Li J, Tang HX, Yu QM, Liu YY & Liu YP, Prenylated coumarins from the fruits of *Artocarpus heterophyllus* with their potential anti-inflammatory and anti-HIV activities. *Nat Prod Res*, 36 (2022) 2526.

26 Otsuki K, Hosoya C, Takamiya R, Kimura M, Kikuchi T, Huang L, Chen CH & Li W, Anti-HIV diterpenoids from *Daphne pseudomezereum*. *Phytochemistry*, 232 (2025) 114366.

27 Zhou L, Zhao CL, Xu CY, Dong MH, Ye JH, Zhang JJ, Pan LT, Zou J & Zhang HJ, Abietane diterpenoids from *Isodon amethystoides* and their biological activities. *Phytochemistry*, 225 (2024) 114171.

28 Jelfs KE & Cooper AI, Molecular simulations to understand the packing and properties of porous molecular materials. *Curr Opin Solid State Mater Sci*, 17 (2013) 19.

29 Kohn W, Becke AD & Parr RG, Density functional theory of electronic structure. *J Phys Chem*, 100 (1996) 12974.

30 Geerlings P, De Proft F & Langenaeker W, Conceptual density functional theory. *Chem Rev*, 103 (2003) 1793.

31 Foresman JB & Frisch AE, Exploring Chemistry with Electronic Structure Methods, 2nd edn, Gaussian Inc (Pittsburgh) 1996.

32 Iczkowski RP & Margrave JL, Electronegativity. *J Am Chem Soc*, 83 (1961) 3547.

33 Parr RG, Donnelly RA, Levy M & Palke WE, Electronegativity: The density functional viewpoint. *J Chem Phys*, 68 (1978) 3801.

34 Parr RG & Pearson RG, Absolute hardness: Companion parameter to absolute electronegativity. *J Am Chem Soc*, 105 (1983) 7512.

35 Maynard AT, Huang M, Rice WG & Covell DG, Reactivity of HIV-1 nucleocapsid protein p7-1 and its zinc finger domain with aromatic disulfides. *Proc Natl Acad Sci U S A*, 95 (1998) 11578.

36 Parr RG, Szentpály LV & Liu S, Electrophilicity index. *J Am Chem Soc*, 121 (1999) 1922.

37 Galano A, Relative antioxidant efficiency of a large series of flavonoids and related compounds. *J Phys Chem B*, 111 (2007) 12898.

38 Gázquez JL, Cedillo A & Vela A, Electrodonating and electroaccepting powers. *J Phys Chem A*, 111 (2007) 1966.

39 Martínez A, Rodríguez-Gironés MA, Barbosa A & Costas M, Donator acceptor map and the role of electron transfer in the antioxidant activity of quercetin. *J Phys Chem A*, 112 (2008) 9037.

40 Roy RK & Saha S, Studies of regioselectivity and reactivity descriptors in conceptual density functional theory. *Annu Rep Sect C Phys Chem*, 106 (2010) 118.

41 Parr RG & Yang W, Density functional approach to the frontier-electron theory of chemical reactivity. *J Am Chem Soc*, 106 (1984) 4049.

42 Nalewajski RF & Parr RG, Legendre transforms and Maxwell relations in density functional theory. *J Chem Phys*, 77 (1982) 399.

43 Roy RK, Krishnamurti S, Geerlings P & Pal S, Local softness and hardness based reactivity descriptors for predicting regioselectivity: A comparison with the Fukui function. *J Phys Chem A*, 102 (1998) 3746.

44 Chattaraj PK & Roy DR, Update 1 of: Electrophilicity index. *Chem Rev*, 107 (2007) PR46.

45 Ghosh SK & Berkowitz M, A classical fluid-like approach to the calculation of local softness and hardness. *J Chem Phys*, 83 (1985) 2976.

46 Cárdenas C, Tiznado W, Ayers PW & Fuentealba P, The Fukui potential. *J Phys Chem A*, 115 (2011) 2325.

47 Morell C, Grand A & Toro-Labbé A, New dual descriptor for chemical reactivity. *J Phys Chem A*, 109 (2005) 205.

48 Chattaraj PK & Giri S, Electrophilicity index within a conceptual DFT framework. *Annu Rep Sect C Phys Chem*, 105 (2009) 13.

49 Frisch MJ, Trucks GW, Schlegel HB, Scuseria GE, Robb MA, Cheeseman JR, Scalmani G, Barone V, Mennucci B, Petersson GA, Nakatsuji H, Caricato M, Li X, Hratchian HP, Izmaylov AF, Bloino J, Zheng G, Sonnenberg JL, Hada M, Ehara M, Toyota K, Fukuda R, Hasegawa J, Ishida M, Nakajima T, Honda Y, Kitao O, Nakai H, Vreven T, Montgomery JA Jr, Peralta JE, Ogliaro F, Bearpark MJ, Heyd JJ, Brothers E, Kudin KN, Staroverov VN, Kobayashi R, Normand J, Raghavachari K, Rendell A, Burant JC, Iyengar SS, Tomasi J, Cossi M, Rega N, Millam JM, Klene M, Knox JE, Cross JB, Bakken V, Adamo C, Jaramillo J, Gomperts R, Stratmann RE, Yazyev O, Austin AJ, Cammi R, Pomelli C, Ochterski JW, Martin RL, Morokuma K, Zakrzewski VG, Voth GA, Salvador P, Dannenberg JJ, Dapprich S, Daniels AD, Farkas O, Foresman JB, Ortiz JV, Cioslowski J & Fox DJ, Gaussian 09, Revision A.1. Gaussian Inc (Wallingford, CT) 2009.

50 Becke AD, Density-functional thermochemistry. III. The role of exact exchange. *J Chem Phys*, 98 (1993) 5648.

51 Lee C, Yang W & Parr RG, Development of the Colle-Salvetti correlation-energy formula into a functional of the electron density. *Phys Rev B*, 37 (1988) 785.

52 Petersson GA & Al-Laham MA, A complete basis set model chemistry. II. Open-shell systems and the total energies of the first-row atoms. *J Chem Phys*, 94 (1991) 6081.

53 Geerlings P, De Proft F & Langenaeker W, Conceptual density functional theory. *Chem Rev*, 103 (2003) 1793.

54 Foresman JB & Frisch AE, Exploring Chemistry with Electronic Structure Methods, 2nd edn, Gaussian Inc (Pittsburgh) 1996.

55 Dennington II R, Keith T & Millam J, GaussView, Version 5. Semichem Inc (Shawnee Mission, KS) 2008.

56 Ren J, Chamberlain PP, Stamp A, Short SA, Weaver KL, Romines KR, Hazen R, Freeman A, Ferris RG, Andrews CW, Boone L, Chan JH & Stammers DK, Structural basis for the improved drug resistance profile of new generation benzophenone non-nucleoside HIV-1 reverse transcriptase inhibitors. *J Med Chem*, 51 (2008) 5000.

57 Curreli F, Kwon YD, Zhang H, Scacalossi D, Belov DS, Tikhonov AA, Andreev IA, Altieri A, Kurkin AV, Kwong PD & Debnath AK, Structure-based design of a small molecule CD4-antagonist with broad spectrum anti-HIV-1 activity. *J Med Chem*, 58 (2015) 6909.

58 Daina A, Michielin O & Zoete V, SwissADME: A free web tool to evaluate pharmacokinetics, drug-likeness and medicinal chemistry friendliness of small molecules. *Sci Rep*, 7 (2017) 42717.

59 Banerjee P, Kemmler E, Dunkel M & Preissner R, ProTox 3.0: A webserver for the prediction of toxicity of chemicals. *Nucleic Acids Res*, 52 (2024) W513.

60 O'Boyle NM, Banck M, James CA, Morley C, Vandermeersch T & Hutchison GR, Open Babel: An open chemical toolbox. *J Cheminform*, 3 (2011) 33.

61 Ertl P, Rohde B & Selzer P, Fast calculation of molecular polar surface area as a sum of fragment-based contributions and its application to the prediction of drug transport properties. *J Med Chem*, 43 (2000) 3714.

62 Veber DF, Johnson SR, Cheng HY, Smith BR, Ward KW & Kopple KD, Molecular properties that influence the oral bioavailability of drug candidates. *J Med Chem*, 45 (2002) 2615.

63 Morris GM, Goodsell DS, Huey R & Olson AJ, Distributed automated docking of flexible ligands to proteins: Parallel applications of AutoDock 2.4. *J Comput Aided Mol Des*, 10 (1996) 293.

64 Dallakyan S & Olson AJ, Small-molecule library screening by docking with PyRx. *Methods Mol Biol*, 1263 (2015) 243.